Geosci. Model Dev. Discuss., 8, 5983–6019, 2015
www.geosci-model-dev-discuss.net/8/5983/2015/
doi:10.5194/gmdd-8-5983-2015

Geoscientific Model Development Discussions
Open Access

Adjoint of the Global Eulerian–Lagrangian Coupled Atmospheric transport model (A-GELCA v1.0): development and validation

D. A. Belikov[1,2,3], S. Maksyutov[1], A. Yaremchuk[4], A. Ganshin[3,5], T. Kaminski[6,a], S. Blessing[6], M. Sasakawa[1], and A. Starchenko[3]

[1]National Institute for Environmental Studies, Tsukuba, Japan
[2]National Institute of Polar Research, Tokyo, Japan
[3]Tomsk State University, Tomsk, Russia
[4]N. Andreev Acoustic Institute, Moscow, Russia
[5]Central Aerological Observatory, Dolgoprudny, Russia
[6]FastOpt GmbH, Hamburg, Germany
[a]now at: The Inversion Lab, Hamburg, Germany

Received: 18 May 2015 – Accepted: 6 July 2015 – Published: 28 July 2015

Correspondence to: D. A. Belikov (dmitry.belikov@nies.go.jp)

Published by Copernicus Publications on behalf of the European Geosciences Union.

Abstract

We present the development of the Adjoint of the Global Eulerian–Lagrangian Coupled Atmospheric (A-GELCA) model that consists of the National Institute for Environmental Studies (NIES) model as an Eulerian three-dimensional transport model (TM), and FLEXPART (FLEXible PARTicle dispersion model) as the Lagrangian plume diffusion model (LPDM).

The tangent and adjoint components of the Eulerian model were constructed directly from the original NIES TM code using an automatic differentiation tool known as TAF (Transformation of Algorithms in Fortran; http://www.FastOpt.com), with additional manual pre- and post-processing aimed at improving the performance of the computing, including MPI (Message Passing Interface). As results, the adjoint of Eulerian model is discrete. Construction of the adjoint of the Lagrangian component did not require any code modification, as LPDMs are able to track a significant number of particles back in time and thereby calculate the sensitivity of observations to the neighboring emissions areas. Eulerian and Lagrangian adjoint components were coupled at the time boundary in the global domain.The results are verified using a series of test experiments. The forward simulation shown the coupled model is effective in reproducing the seasonal cycle and short-term variability of CO_2 even in the case of multiple limiting factors, such as high uncertainty of fluxes and the low resolution of the Eulerian model. The adjoint model demonstrates the high accuracy compared to direct forward sensitivity calculations and fast performance. The developed adjoint of the coupled model combines the flux conservation and stability of an Eulerian discrete adjoint formulation with the flexibility, accuracy, and high resolution of a Lagrangian backward trajectory formulation.

GMDD
8, 5983–6019, 2015

1 Introduction

Forecasts of CO_2 levels in the atmosphere and predictions of future climate depend on our scientific understanding of the natural carbon cycle (IPCC, 2007; Peters et al., 2007). To estimate the spatial and temporal distribution of carbon sources and sinks, inverse methods are used to infer carbon fluxes from geographically sparse observations of the atmospheric CO_2 mixing ratio (Tans et al., 1989). The first comprehensive efforts in atmospheric CO_2 inversions date back to the late 1980s and early 1990s (Enting and Mansbridge, 1989; Tans et al., 1989). With the increase in spatial coverage of CO_2 observations and the development of 3-D tracer transport models, a variety of numerical experiments and projects have been performed by members of the so-called "TransCom" community of inverse modelers (e.g., Law et al., 1996, 2008; Denning et al., 1999; Gurney et al., 2002, 2004; Baker et al., 2006; Patra et al., 2011). A number of studies have proposed improvements to the inverse methods of atmospheric transport (Kaminski et al., 1999b; Rödenbeck et al., 2003; Peters et al., 2005; Peylin et al., 2005; Chevallier et al., 2005; Meirink et al., 2008; Maki et al., 2010). Despite progress in atmospheric CO_2 inversions, a recent intercomparison (Peylin et al., 2013) demonstrated the need for further refinement.

In recent decades, a density of observational network established to monitor greenhouse gases in the atmosphere has been increased, and measurements taken onboard ships and aircraft are becoming available (Bovensmann et al., 1999). However, on a global scale CO_2 observation are not existing for many remote regions not covered by networks. This lack of data is one of the main limitations of atmospheric inversions, which can be filled by monitoring from space (Rayner and O'Brien, 2001). The satellite observation data from current (GOSAT, Kuze et al., 2009; Yokota et al., 2009; OCO-2, Crisp et al., 2004) and future missions (CarbonSat/CarbonSat Constellation; Bovensmann et al., 2010; Buchwitz et al., 2013) offer enormous potential for CO_2 inverse modeling. Optimal application of large observed datasets requires expanding the inverse analysis of CO_2 to finer resolution, higher precision and faster performance.

GMDD
8, 5983–6019, 2015

To link surface fluxes of CO_2 to observed atmospheric concentrations, an accurate model of atmospheric transport and an inverse modeling technique are needed. Generally, there are the Eulerian and the Lagrangian method of modelling the atmospheric constituents transport. The Eulerian method treats the atmospheric tracers as a continuum on a control volume basis, so it is more effective in reproducing of long-term patterns, i.e. the seasonal cycle or interhemispheric gradient. The Lagrangian Particle Dispersion Models (LPDMs) consider atmospheric tracers as a discrete phase and tracks each individual particle, therefore LPDMs are better for resolving synoptic and hourly variations.

To relate fluxes and concentrations of a long-lived species like CO_2 a transport model must cover a long simulation period (e.g., Bruhwiler et al., 2005). Therefore, computing time is a critical issue and minimization of the computational cost is essential. If tracer is a chemically inert, the transport can be represented by a model's Jacobian matrix, because the simulated concentration at observational sites is a linear function of the flux sets. To compute such a matrix a transport model is running multiple times with set of prescribed surface fluxes. The adjoint of the transport model is an efficient way to evaluate derivatives of concentration of the simulated tracer at observational locations towards to the sources and sinks of tracer (Kaminski et al., 1999).

Marchuk (1974) first applied the adjoint approach in atmospheric science. After that, this method became widely used in meteorology. In the 1990s the approach was expanded to the field of tracer transport modeling (Elbern et al., 1997; Kaminski et al., 1999). Adjoint models have numerous applications, including the data assimilation of concentrations, inverse modeling of chemical source strengths, sensitivity analysis, and parameter sensitivity estimation (Enting, 2002; Haines et al., 2014). Recent studies have used this method to constrain estimates of the emissions of various tracers using retrieved column integrals from the GOME and MOPITT satellite instruments (Müller and Stavrakou, 2005; Kopacz et al., 2009).

Using the adjoint model speeds the process of inverse modeling. However, high CPU and memory demands prevent us from using Eulerian chemical transport models

GMDD
8, 5983–6019, 2015

(CTMs) with high-resolution grids in inversions. It would be beneficial to increase the model resolution close to observation points, where small uncertainties in the transport can seriously improve optimization of the resulting emission fluxes.

LPDM running in the backward mode can explicitly estimate a source–receptor sensitivity matrix by solving the adjoint equations of atmospheric transport (Stohl et al., 2009), which is mathematically a Jacobian expressing the sensitivity of concentration at observational locations. Marchuk (1995), and Hourdin and Talagrand (2006) discussed the equivalence of the adjoint of forward transport models to backward transport models.

To utilize of the strongest sides of both methods, Lagrangian and Eulerian chemical transport models can be coupled to develop the adjoint, which is suitable for the simultaneous estimation of global and regional emissions. Coupling can be performed in several ways; e.g., a regional-scale LPDM can be coupled to a global Eulerian model at the domain boundary (Rödenbeck et al., 2009; Rigby et al., 2011), or a global-scale LPDM can be coupled to an Eulerian model at the time boundary (Koyama et al., 2011; Thompson and Stohl, 2014).

One goal of this study is to present the development and evaluation of an Adjoint of the Global Eulerian–Lagrangian Coupled Atmospheric model (A-GELCA), which consists of an Eulerian National Institute for Environmental Studies global Transport Model (NIES-TM; Maksyutov et al., 2008; Belikov et al., 2011, 2013a, b) and a Lagrangian particle dispersion model (FLEXPART; Stohl et al., 2005). This approach utilizes the accurate transport of the LPDM to calculate the signal near to the receptors, and rapid calculation of background responses using the adjoint of the Eulerian global transport model. In contrast to previous works (Rödenbeck et al., 2009; Rigby et al., 2011; Thompson and Stohl, 2014), in which the regional models were coupled at the spatial boundary of the domain, we implemented a coupling at the time boundary in the global model domain.

The remainder of this paper is organized as follows. An overview of the coupled model is provided in Sect. 2, and in Sect. 3 we describe the variational inversion pro-

GMDD
8, 5983–6019, 2015

cess. In Sect. 4 we address several problems regarding the coupled model that have not been covered previously (Ganshin et al., 2012). In Sect. 5 we describe the formulation and evaluation of the adjoint model. The computational efficiency of the adjoint model is analyzed in Sect. 6, and finally the conclusions are presented in Sect. 7.

2 Model and method

2.1 Global coupled Eulerian–Lagrangian model

In the paper we use a global Eulerian–Lagrangian coupled model, the principles of which are described by Ganshin et al. (2012). In this section we provide the formula in its discrete form, as implemented in the model for the case of surface fluxes:

$$C(x_r,t_r) = \frac{T m_{\mathrm{air}}}{hNL\rho m_{\mathrm{CO_2}}} \sum_{ij}^{IJ} \sum_{l=0}^{L} F_{ij}^{l} \sum_{n=1}^{N} f_{ij}^{\mathrm{In}} + \frac{1}{N} \sum_{ijk}^{IJK} C_{ijk}^{\mathrm{B}} \sum_{n=1}^{N} f_{ijk}^{n}, \quad (1)$$

where i, j, and k are the indices that characterize the position of the particle in the cell; l is the time index; p is the particle index; F_{ij}^{l} are the surface fluxes in $\mathrm{kg\,m^{-2}\,s^{-1}}$; C_{ijk}^{B} are the background concentrations in the Eulerian model; f_{ijk}^{n} equals unity if the particle is within cell i,j,k, otherwise it equals zero; T is the duration of the trajectory; L is the number of steps in time; N is the total number of particles; h is the height up to which the effect of the surface fluxes is considered significant; ρ is the average air density below height h; and m_{air} and $m_{\mathrm{CO_2}}$ are the molar masses of air and carbon dioxide, respectively. The FLEXPART model starts at the observation point and calculates seven days' worth of backward trajectories for 1000 air particles, which are dispersed under the influence of turbulent diffusion. The background grid values of the concentrations, which are interpolated to the final points of the back trajectories, are transferred to the observation point and are the second term in the right-hand side of Eq. (1). The first term in this formula describes the contribution of the sources of the component considered; these sources are located along the trajectories inside layer

GMDD
8, 5983–6019, 2015

h (500 m). The value of the first term is proportional to the flux in each cell along the trajectory, and to the time during which the air particle is inside this cell (Ganshin et al., 2013). We implemented a coupling at the time boundary in the global domain.

The coupled model consists of FLEXPART (version 8.0; run in backward mode) as the Lagrangian particle dispersion model, and NIES TM (version NIES-08.1i) as the Eulerian off-line global transport model to calculate the background CO_2 values.

2.2 NIES transport model

Since the first publication of the GELCA model in 2012, the NIES transport model has undergone significant updates. We provide a brief outline of the major features of the current model. NIES TM is a global three-dimensional CTM that simulates the global distribution of atmospheric tracers between the Earth's surface and a pressure level of 5 hPa. The model's employs the standard horizontal latitude–longitude grid with reduced number of meshes towards the poles and a spatial resolution of $2.5^\circ \times 2.5^\circ$ near the equator (Belikov et al., 2011). The vertical coordinate is a flexible hybrid sigma–isentropic (σ–θ) with 32 levels (Belikov et al., 2013b). To parameterize turbulent diffusivity we follows the method proposed by Hack et al. (1993), with a separate evaluation of transport processes in free troposphere and the planetary boundary layer (PBL). The PBL heights are provided by the European Centre for Medium-Range Weather Forecasts (ECMWF) ERA-Interim reanalysis. The modified Kuo-type parameterization scheme is used for cumulus convection (Belikov et al., 2013a).

Inverse modeling assumes that the model reasonably well reproduces the relationship between atmospheric mixing ration and surface fluxes, assuming that the biases between the simulated and observed concentrations are mostly due to the emission inventories errors. To ensure that this is the case, the NIES TM model has been evaluated extensively, and it consistently performs well in intercomparisons against SF_6 and CO_2 (Belikov et al., 2011, 2013b), CH_4 (Patra et al., 2011; Belikov et al., 2013b), and ^{222}Rn (Belikov et al., 2013a) measurements.

GMDD
8, 5983–6019, 2015

2.3 FLEXPART

FLEXPART similar to other LPDMs consider atmospheric tracers as a discrete phase and tracks pathways of each individual particle. The advantage of this approach is direct estimation the sensitivity of measurements to the neighboring sink and sources by running the particles back in time. Usually it is enough to simulate for a limited number of days (2–10) to determine, where particles intercept the surface layer.

2.4 Meteorological data

To run both models we use reanalysis which combines the Japanese 25 yr Reanalysis (JRA-25) and the Japanese Meteorological Agency Climate Data Assimilation System (JCDAS) dataset (Onogi et al., 2007). The JRA-25/JCDAS dataset is distributed on a Gaussian grid T106 with horizontal resolution $1.25^{\circ} \times 1.25^{\circ}$, 40 sigma-pressure levels and in 6 h time steps. The use of JRA-25/JCDAS data for Eulerian and Lagrangian models provides a consistency in the calculated fields; however, some features of FLEXPART and NIES TM require different methods for processing the meteorological data.

2.4.1 Meteorological data processing for NIES TM

Isolation of the transport equations is an effective way to save a significant amount of CPU time during tracer transport simulation. At the preprocessing stage, the NIES TM core produced a static archive of advective, diffusive, and convective mass fluxes with time step similar to the one of original JRA-25/JCDAS data (6 h). After that the archive is used by an "offline" model specially designed only for passive transport of tracer. Intermediate fluxes are derived by interpolation.

Besides the mass fluxes, the static archives contain fields of temperature, pressure, humidity, vertical grid parameters (variation of the sigma-isentropic vertical coordinate over time), and others. The pre-calculated and stored data field can be used directly for any of the inert tracers. It is also possible to simulate chemically active tracers

GMDD
8, 5983–6019, 2015

if the chemical reaction can be written in the simplified form; e.g., for ^{222}Rn, CH_4. Approximately 20 3-dimensional and 1-dimensional arrays are written to a hard disk for every record. This comprises around 10 GB of data per month for the model's standard resolution of 2.5° × 2.5°.

2.4.2 Meteorological data processing for FLEXPART

Originally, FLEXPART was driving by ECMWF reanalysis dataset distributed on a grid with regular latitude–longitude horizontal structure and sigma–pressure vertical coordinate. Current version of the model was adapted to use JRA-25/JCDAS data, by horizontal bilinear interpolation of the required parameters from a Gaussian grid to a regular 1.25 × 1.25 grid. The vertical structure and temporal resolution of of JRA-25/JCDAS data were used without modification.

Given large differences in structure, resolution and parameter estimation method used in different reanalysis dataset the use of the same meteorology for both Eulerian and Lagrangian models is a significant benefit.

3 Inverse modeling for the flux optimization problem

Although the variational inversion method theory for minimizing the discrepancy between modeled and observed mixing ratios has been well described and published (i.e. Chevallier et al., 2005), we summarize it here.

The aim of the inverse problem is to find the value of a state vector $\boldsymbol{x}$ with n elements that minimizes a cost function $J(x)$ using a least-squares method:

$$J(\boldsymbol{x}) = \frac{1}{2}(\boldsymbol{x}-\boldsymbol{x}_b)^T\mathbf{B}^{-1}(\boldsymbol{x}-\boldsymbol{x}_b) + \frac{1}{2}(\mathbf{H}\boldsymbol{x}-\boldsymbol{y})^T\mathbf{R}^{-1}(\mathbf{H}\boldsymbol{x}-\boldsymbol{y}), \quad (2)$$

where $\boldsymbol{y}$ is a vector of observations with m elements, and the matrix $\mathbf{H}$ represents the forward model simulation mapping the state vector $\boldsymbol{x}$ to the observation space. Here, $\mathbf{R}$

GMDD
8, 5983–6019, 2015

is the covariance matrix (size $m \times m$) for observational error, which includes instrument and representation errors. The matrix **R** also includes errors of the forward model **H**. **B** is the covariance matrix (size $n \times n$) of error for prior information of the state vector $\boldsymbol{x}_b$. Use of the cost function in the form of Eq. (2) assumes that all errors must have Gaussian statistics and be unbiased (Rodgers, 2000).

For linear **H**, Eq. (2) has an analytic solution involving a matrix inversion. If the Jacobian **H** is available this analytic solution can implemented, unless the matrix sizes are too large for the available computing resources. Alternatively, Eq. (2) can be solved through an iterative minimization algorithm. In this case, the existence of the gradient of $J(x)$ with respect to x allows using of powerful gradient algorithms for minimisation. This gradient is efficiently provided by the adjoint (Giering and Kaminski, 1998; Kaminski et al., 1999; Chevallier et al., 2005; Kopacz et al., 2009).

4 Assessment of the coupled model

The effect of different horizontal resolutions on Eulerian models is discussed in detail by Patra et al. (2008). In general, higher resolution helps to resolve a more detailed distribution of the tracer. However, the use of a more detailed grid leads to additional computational cost, which is not always justified by the resulting model output. This is largely due to the limited availability of high-resolution meteorology and tracer emission datasets.

Ganshin et al. (2012) in various test showed that the coupled model surpasses the Eulerian model in 4-month simulations. The advantage of GELCA in reproducing the high-concentration spikes and short-term variations caused mainly by anthropogenic emissions is more vivid with use of high resolution (1 km × 1 km) surface fluxes compared to standard low-resolution (1° × 1°) fluxes.

We repeated the comparison undertaken by Ganshin et al. (2012) for a two-year period using an updated set of prescribed fluxes, which combines four components similar to analysis performed by Takagi et al. (2011) and Maksyutov et al. (2012):

GMDD
8, 5983–6019, 2015

(a) anthropogenic fluxes from the Open source Data Inventory of Anthropogenic CO_2 (ODIAC; Oda and Maksyutov, 2011) and the Carbon Dioxide Information Analysis Center's (CDIAC; Andres et al., 2009, 2011) datasets, (b) biosphere fluxes simulated by the Vegetation Integrative SImulator for Trace gases (VISIT) terrestrial biosphere model (Ito, 2010; Saito et al., 2011, 2013), (c) oceanic fluxes predicted by data assimilation system based on the Offline ocean Tracer Transport Model (OTTM; Valsala and Maksyutov, 2010); and (d) biomass burning emissions from the Global Fire Emissions Database (GFED) version 3.1 (van der Werf et al., 2010). Biosphere fluxes have daily time step, while others are monthly.

We considered several cases with different model resolutions. For NIES TM we tested grids at 10.0, 2.5, and 1.25° resolutions, with FLEXPART running at 1.0° (Table 1). The resolution of the input fluxes was matched to that of FLEXPART. Modeled results were compared with the Siberian observations obtained by the Center for Global Environmental Research (CGER) of the National Institute for Environmental Studies (NIES) and the Russian Academy of Science (RAS), from seven tower sites (JR-STATION) as described in Table 2 (Sasakawa et al., 2010).

Siberia is assumed to be a substantial source and sink of CO_2 emissions, with high uncertainties in the fluxes describing them (McGuire et al., 2009; Hayes et al., 2011; Saeki et al., 2013). As a result, CTMs tend to reproduce the interseasonal variability of CO_2 quite poorly.

Figures 2 and 3 compare the coupled and Eulerian model results with tower observations from Igrim and Vaganovo. Recent modifications (Sect. 2.2) mean that the performance of NIES TM is significantly improved compared with the results reported by Ganshin et al. (2012). However, in this case the coupled model reproduces the observations better than the Eulerian model used on its own, providing a better simulation of the seasonal variation and its amplitude. The standard deviation of the coupled model misfit to the observations is around 0.5 ppm smaller. Moreover, the version of the coupled model with a very coarse grid of NIES TM (10.0°) outperforms the higher-resolution versions of the Eulerian model (Table 3). Given the huge difference in com-

GMDD
8, 5983–6019, 2015

putation costs between NIES TM for low- and high-resolution grids (i.e. a difference by a factor of ∼ 15 between grids with resolution 10.0 and 2.5°), the advantage of the GELCA model is clear. Performance is important, as the setup considered here is almost identical to the case used in the inverse modeling of CO_2.

This case shows that the coupled model is effective even in the case of multiple limiting factors, such as high uncertainty of fluxes, a small number of observations, and the low resolution of the Eulerian model. We recognize that the use of the concentrations simulated from the highly uncertain surface fluxes to judge the quality of different model configurations is quite problematic. Nevertheless, we cannot improve our analysis, because we do not have concentration measurements for tracers with more accurate fluxes, like SF_6.

5 Construction and validation of the adjoint model

5.1 Construction

In this section, we present the development of the adjoint of the coupled model. Construction of the adjoint to the Lagrangian part does not require any modification to the code, as LPDMs are able to track a significant number of particles backwards in time and thereby calculate the sensitivity of observations to the neighboring emissions areas.

The development of the adjoint to the Eulerian part is more complicated. We decided to develop a discrete adjoint of NIES TM in order to make it consistent with the forward model. An alternative approach is a construction of continuous adjoint derived from the leading equations of the forward model (Giles and Pierce, 2000). The main advantage of the discrete adjoint model is that the resulting gradients of the numerical cost function are exact, even for nonlinear or iterative algorithms, making them easier to validate, as validation of the adjoint model is an essential and complicated task.

GMDD
8, 5983–6019, 2015

The tangent linear and adjoint models for NIES TM were created using the Transformation of Algorithms in Fortran (TAF) software (http://www.FastOpt.com). Use of this tool required some manual treatment of the code. We often manually redesign and optimize the automatically generated adjoint code to optimize the efficiency and improve readability and clarity of the adjoint model.

The advantages of our coupled adjoint model are as follows.

1. Simple construction of the Lagrangian part of the adjoint, as modification of LPDM is not required. Potentially, NIES TM can be coupled to any Lagrangian model.

2. Minimizing of the simulation time can be obtained, as once calculated output from the Lagrangian model is applicable for different long-lived tracers.

3. Reduction of aggregation errors can be achieved, as the sensitivity for small regions and even individual model cells near to observation sites is estimated using the LPDM part, while the sensitivity for large regions remoted from the monitoring sites is derived using the Eulerian part (Kaminski et al., 2001).

4. Minimizing of the computational cost can be obtained, as high-resolution simulation are performed over limited number of regions nearby to the observational sites using the LPDM part, while for the rest of the globe the coarse-resolution results are calculated by the Eulerian part.

5. High consistency of calculated tracer field calculated by Lagrangian and Eulerian models due to use of the same impute meteorology.

5.2 Validation of the coupled adjoint

An essential stage of the adjoint model construction is validation. A lack of accuracy in the adjoint model is likely to degrade the performance of the minimisation of Eq. (2). Several different tests were carried out to evaluate the accuracy and precision of the adjoint model calculation. Considering a simple formulation of the adjoint for the Lagrangian part, we focused on testing the NIES TM adjoint.

GMDD
8, 5983–6019, 2015

5.2.1 Validation of the NIES TM adjoint

The discrete adjoint obtained through automatic differentiation can be easily validated by comparing the adjoint sensitivities with forward model gradients calculated using the finite difference approximation (Henze et al., 2007).

Forward model sensitivity, λ, is calculated using the one- or two-sided finite difference equation,

$$\lambda = \frac{M'(x+\varepsilon) - M'(x)}{\varepsilon} \tag{3}$$

$$\lambda = \frac{M'(x+\varepsilon) - M'(x-\varepsilon)}{2\varepsilon} \tag{4}$$

where M' denotes the tangent linear model. A range of $\varepsilon = 0.1$–0.01 proved in most cases to give an optimal balance between truncation and roundoff error (Henze at al., 2007).

In the first test, forward simulations were carried out with an initial CO_2 distribution and zero surface flux for 2 days using a horizontal grid with resolution $2.5^\circ \times 2.5^\circ$. Adjoint simulations were then performed with CO_2 distribution perturbed by 1 ppm per grid cell. The adjoint gradient was then compared with that from the finite difference calculated using Eq. (3) in order to save CPU time by minimizing the number of forward model function calculation for the case $\varepsilon = 0.01$.

To quantify the difference between the two calculations of sensitivity λ we define the local relative error

$$E(\mathrm{lon}, \mathrm{lat}) = \frac{|\lambda_A - \lambda_F|}{\max \lambda_A}, \tag{5}$$

where the subscripts A and F refer to adjoint and finite difference respectively, lon, lat – longitude and latitude correspondently. Figure 3c shows $E(\mathrm{lon}, \mathrm{lat})$ with a logarithmic color scale. The sensitivities obtained by the adjoint have maximum relative error

GMDD
8, 5983–6019, 2015

of order 10^{-16}, indicating that transport in the NIES TM adjoint is correct over short timescales. The overall comparisons did not seriously changed if we select a different grid cells or use various values of ε.

The definition of the adjoint model M^* requires that for an inner product $\langle , \rangle$ and two random vectors $\boldsymbol{u}$ and $\boldsymbol{v}$, the following expression should be valid:

$$\forall \boldsymbol{u}, \forall \boldsymbol{v} \langle M' \boldsymbol{u}, \boldsymbol{v} \rangle = \langle \boldsymbol{u}, M^* \boldsymbol{v} \rangle. \tag{6}$$

For practical use the identity in Eq. (6) is reworded as follows (Wilson et al., 2014):

$$\frac{\|M'(\boldsymbol{u})\|^2}{(\boldsymbol{u} M^*(M(\boldsymbol{u})))} = 1. \tag{7}$$

We use Eq. (7) to test the adjoint model initialized using several different random setups. For all cases, Eq. (7) compares well with machine epsilon.

5.2.2 Real case simulation

The next series of calculations was made for real measurements. As in the first part of the article, we used data from the Siberian observation network (Table 2) for the period 01–04 January 2010. The NIES adjoint was simulated with a horizontal resolution of $2.5^\circ \times 2.5^\circ$, and the Lagrangian response was simulated with a horizontal resolution of $1.0^\circ \times 1.0^\circ$.

Figure 4 shows the sensitivity calculated with the Eulerian component, while Fig. 5 shows the same but using the Lagrangian component. Although the contours of the two figures coincide, it is clear that the Eulerian adjoint has a wider footprint, with the greatest value in an area where the effect of all stations is summed. In this case, most of the stations can be outside this zone, as the Euler model monitors large-scale changes. This figure illustrates why the Eulerian model, even with a sufficiently detailed grid, is unable to reproduce CO_2 variations (Sect. 4). The footprint width increases with resolution.

GMDD
8, 5983–6019, 2015

The FLEXPART model sensitivity shows more irregular distributions, and higher values closer to the observational sites, thereby reflecting the model's ability to monitor small-scale changes.

During coupling, the sensitivity is aligned due to the crosslinking of components (Fig. 6). Thus, intensity has a maximum near the stations and smoothly decreases with increasing distance. The Eulerian and Lagrangian models employ different approaches and grid resolutions for the modeling of atmospheric tracers, and can thus resolve processes with different time and spatial scales, and underlying physics.

Figure 7 shows the sensitivity calculated for the same setup as for Fig. 6, but using NIES TM with a 10.0° resolution. By changing the Eulerian model resolution, it is possible to change size of the footprint. This system can utilize responses calculated at higher resolutions, such as 0.5 or 0.1°, but these setups require more accurate driving data and regular observations available for smaller time steps.

6 Computational efficiency

We tested several different methods to reduce the computational burden of the adjoint model. First, the Eulerian part of the adjoint model was driven by static archives of meteorological parameters, as described in Sect. 2.4.1. Second, the forward NIES model was altered so that at each model timestep it saved any variables that would also be needed by the adjoint model. These variables therefore did not have to be recalculated for use in the adjoint model. (This was possible because we used a discrete version of the adjoint, which was fully compatible with the forward model.) Third, the Lagrangian part of the adjoint model made use of pre-calculated response functions, as described in Sect. 2.4.2.

To run the adjoint model we used a Linux workstation with 8 Intel(R) Xeon(R) E5-4650 2.70 GHz processors and 64 GB of RAM. The CPU time of the adjoint model (backward only) is almost equal to CPU time required to run the forward model. It takes about 1.3 min for a weeklong iteration (forward and backward). The memory demand

GMDD
8, 5983–6019, 2015

is about 1 GB. Henze et al. (2007) reports that the ratio between simulation time in backward and forward modes for adjoint models derived for other CTMs, as follows: GEOS-Chem: 1.5, STEM: 1.5, CHIMERE: 3–4, IM-AGES: 4, Polair: 4.5–7, and CIT: 11.75. Thus, the adjoint of the developed coupled model is quite efficient. To achieve this level of efficiency, a substantial amount of manual programming effort is required, despite the automatic code generated by TAF. The main disadvantage of TAF is that many redundant recomputations are often generated by the compiler. A crucial optimization of the adjoint code is required to eliminate these extra recomputations.

7 Summary

In this papers we have presented the construction and evaluation of an adjoint of the global Eulerian–Lagrangian coupled model that will be integrated into a variational inverse system designed to optimizing surface fluxes. The coupled model combines the NIES three-dimensional transport model as its Eulerian part and the FLEXPART plume diffusion model as its Lagrangian component. The model was originally developed to study the carbon dioxide and methane atmospheric distribution.

FLEXPART is tracking a significant number of particles back in time, and thereby calculates the sensitivity of observations to the neighboring emissions areas. Thus, construction of the adjoint to the Lagrangian part does not require any modification to the code.

For Eulerian part the discrete adjoint was constructed directly from the original NIES TM code, in contrast to a construction of continuous adjoint derived from the forward model basic equations. The tangent and adjoint models of the Eulerian model were derived using the automatic differentiation software TAF (http://www.FastOpt.com), which significantly accelerated the development. However, considerable manual processing of forward and adjoint model codes was necessary to improve transparency of the model and to optimize the performance of computing, including MPI. The TAF code used here (version 1.5) did not fully support MPI routines.

GMDD
8, 5983–6019, 2015

The Eulerian and Lagrangian adjoints were coupled at the time boundary in the global domain. The main benefit of the developed discrete adjoint is accurate calculation of the numerical cost function gradients, even if the algorithms are nonlinear. The overall advantages of the developed model also include relatively simple construction of the adjoint to the Lagrangian part and computation using the Lagrangian component, scalability of sensitivity calculation depending on distance to monitoring sites, thereby reducing aggregation errors, and computational efficiency even for high-resolution simulations.

The accuracy of the transport scheme of the forward coupled model was investigated using simulation of distribution of the atmospheric CO_2. The GELCA components and the model itself had previously been validated in various tests and by comparison with both measurements and other transport models for CO_2 and other tracers. Performed in the paper analyses showed, that GELCA is effective in capturing the seasonal variability of atmospheric tracer at observation sites. Decreasing of the Eulerian model resolution are not able to significantly distort the transport model performance, however, running the coupled model using NIES TM with low resolution grid can maximize simulation speed and use of data storage.

The Eulerian and Lagrangian components of the adjoint model were validated using various tests in which the adjoint gradients were compared to gradients calculated with numerical finite difference. We evaluated each individual routine of discrete adjoint of Eulerian model and the adjoint gradients of the cost function. The obtained precision of the results in considered numerical experiments demonstrates proper construction of the adjoint.

The CPU time of the adjoint model is comparable with that of other models, as we used several methods to reduce the computational load. The forward NIES model was altered so that at each model timestep it saved any variables that would also be needed by the adjoint model. These variables therefore did not have to be recalculated for use in the adjoint model. In addition, the adjoint simulation was isolated from the recalculation of NIES TM meteorological parameters and Lagrangian response functions.

GMDD
8, 5983–6019, 2015

All supplementary parameters are pre-calculated before running the adjoint and are stored in static archives.

The developed adjoint model will be incorporated into variation inversion system aiming studying greenhouse gases (mainly CH_4 and CO_2), by assimilating tracer measurements from in situ, aircraft and remote sensing observations. However, before performing real inverse modeling simulations it is necessary to select a proper minimization program and find the error covariance matrices **R** and **B** with the optimal values.

Code availability

All code in the current version of the NIES forward model is available on request. Any potential user interested in these modules should contact D. A. Belikov, and any feedback on the modules is welcome. Note that one may need help using the forward and adjoint model effectively, but open support for the model is not available due to lack of resources. The code of the adjoint part of the current NIES model is unavailable for distribution, as it was generated using the commercial tool TAF (http://www.FastOpt.com). However, we can provide the sources which were used as input for TAF.

The FLEXPART code was taken from the official web site http://flexpart.eu/. The procedures necessary to run FLEXPART with the JCDAS reanalysis are also available upon request.

Acknowledgements. The authors thank A. Stohl for providing the FLEXPART model. We also thank T. Machida for Siberian observation data (downloaded from http://db.cger.nies.go.jp/). The JRA-25/JCDAS meteorological datasets used in the simulations were provided by the Japan Meteorological Agency. The computational resources were provided by NIES. This study was performed by order of the Ministry for Education and Science of the Russian Federation No. 5.628.2014/K and was supported by The Tomsk State University Academic D. I. Mendeleev Fund Program in 2014–2015 and by GRENE Arctic project.

GMDD
8, 5983–6019, 2015

References

Andres, R. J., Boden, T. A., and Marland, G.: Annual Fossil-Fuel CO_2 Emissions: Mass of Emissions Gridded by One Degree Latitude by One Degree Longitude, Carbon Dioxide Information Analysis Center, Oak Ridge National Laboratory, U.S. Department of Energy, Oak Ridge, Tenn., USA, doi:10.3334/CDIAC/ffe.ndp058.2009, 2009.

Andres, R. J., Gregg, J. S., Losey, L., Marland, G., anmd Boden, T.: Monthly, global emissions of carbon dioxide from fossil fuel consumption, Tellus B, 63, 309–327, 2011.

Baker, D. F., Law, R. M., Gurney, K. R., Rayner, P., Peylin, P., Denning, A. S., Bousquet, P., Bruhwiler, L., Chen, Y.-H., Ciais, P., Fung, I. Y., Heimann, M., John, J., Maki, T., Maksyutov, S., Masarie, K., Prather, M., Pak, B., Taguchi, S., and Zhu, Z.: TransCom 3 inversion intercomparison: impact of transport model errors on the interannual variability of regional CO_2 fluxes, 1988–2003, Global Biogeochem. Cy., 20, GB1002, doi:10.1029/2004GB002439, 2006.

Belikov, D., Maksyutov, S., Miyasaka, T., Saeki, T., Zhuravlev, R., and Kiryushov, B.: Mass-conserving tracer transport modelling on a reduced latitude-longitude grid with NIES-TM, Geosci. Model Dev., 4, 207–222, doi:10.5194/gmd-4-207-2011, 2011.

Belikov, D. A., Maksyutov, S., Krol, M., Fraser, A., Rigby, M., Bian, H., Agusti-Panareda, A., Bergmann, D., Bousquet, P., Cameron-Smith, P., Chipperfield, M. P., Fortems-Cheiney, A., Gloor, E., Haynes, K., Hess, P., Houweling, S., Kawa, S. R., Law, R. M., Loh, Z., Meng, L., Palmer, P. I., Patra, P. K., Prinn, R. G., Saito, R., and Wilson, C.: Off-line algorithm for calculation of vertical tracer transport in the troposphere due to deep convection, Atmos. Chem. Phys., 13, 1093–1114, doi:10.5194/acp-13-1093-2013, 2013a.

Belikov, D. A., Maksyutov, S., Sherlock, V., Aoki, S., Deutscher, N. M., Dohe, S., Griffith, D., Kyro, E., Morino, I., Nakazawa, T., Notholt, J., Rettinger, M., Schneider, M., Sussmann, R., Toon, G. C., Wennberg, P. O., and Wunch, D.: Simulations of column-averaged CO_2 and CH_4 using the NIES TM with a hybrid sigma-isentropic (σ-θ) vertical coordinate, Atmos. Chem. Phys., 13, 1713–1732, doi:10.5194/acp-13-1713-2013, 2013b.

Bovensmann, H., Burrows, J. P., Buchwitz, M., Frerick, J., Noël, S., Rozanov, V. V., Chance, K. V., and Goede, A. P. H.: SCIAMACHY: mission objectives and measurement modes, J. Atmos. Sci., 56, 127–150, 1999.

Bovensmann, H., Buchwitz, M., Burrows, J. P., Reuter, M., Krings, T., Gerilowski, K., Schneising, O., Heymann, J., Tretner, A., and Erzinger, J.: A remote sensing technique for global

GMDD
8, 5983–6019, 2015

monitoring of power plant CO_2 emissions from space and related applications, Atmos. Meas. Tech., 3, 781–811, doi:10.5194/amt-3-781-2010, 2010.

Bruhwiler, L. M. P., Michalak, A. M., Peters, W., Baker, D. F., and Tans, P.: An improved Kalman Smoother for atmospheric inversions, Atmos. Chem. Phys., 5, 2691–2702, doi:10.5194/acp-5-2691-2005, 2005.

Buchwitz, M., Reuter, M., Bovensmann, H., Pillai, D., Heymann, J., Schneising, O., Rozanov, V., Krings, T., Burrows, J. P., Boesch, H., Gerbig, C., Meijer, Y., and Löscher, A.: Carbon Monitoring Satellite (CarbonSat): assessment of atmospheric CO_2 and CH_4 retrieval errors by error parameterization, Atmos. Meas. Tech., 6, 3477–3500, doi:10.5194/amt-6-3477-2013, 2013.

Chevallier, F., Fisher, M., Peylin, P., Serrar, S., Bousquet, P., Bréon, F.-M., Chédin, A., and Ciais, P.: Inferring CO_2 sources and sinks from satellite observations: method and application to TOVS data, J. Geophys. Res., 110, D24309, doi:10.1029/2005JD006390, 2005.

Crisp, D., Atlas, R. M., Bréon, F.-M., Brown, L. R., Burrows, J. P., Ciais, P., Connor, B. J., Doney, S. C., Fung, I. Y., Jacob, D. J., Miller, C. E., O'Brien, D., Pawson, S., Randerson, J. T., Rayner, P., Salawitch, R. S., Sander, S. P., Sen, B., Stephens, G. L., Tans, P. P., Toon, G. C., Wennberg, P. O., Wofsy, S. C., Yung, Y. L., Kuang, Z., Chudasama, B., Sprague, G., Weiss, P., Pollock, R., Kenyon, D., and Schroll, S.: The Orbiting Carbon Observatory (OCO) mission, Adv. Space Res., 34, 700–709, 2004.

Elbern, H., Schmidt, H., and Ebel, A.: Variational data assimilation for tropospheric chemistry modeling, J. Geophys. Res., 102, 15967–15985, 1997.

Enting, I. G. and Mansbridge, J. V.: Seasonal sources and sinks of atmospheric CO_2: direct inversion of filtered data, Tellus B, 41, 111–126, doi:10.1111/j.1600-0889.1989.tb00129.x, 1989.

Enting, I. T.: Inverse Problems in Atmospheric Constituent Transport, Cambridge University Press, Cambridge, UK, 2002.

Ganshin, A., Oda, T., Saito, M., Maksyutov, S., Valsala, V., Andres, R. J., Fisher, R. E., Lowry, D., Lukyanov, A., Matsueda, H., Nisbet, E. G., Rigby, M., Sawa, Y., Toumi, R., Tsuboi, K., Varlagin, A., and Zhuravlev, R.: A global coupled Eulerian-Lagrangian model and 1×1 km CO_2 surface flux dataset for high-resolution atmospheric CO_2 transport simulations, Geosci. Model Dev., 5, 231–243, doi:10.5194/gmd-5-231-2012, 2012.

Giering, R. and Kaminski, T.: Recipes for adjoint code construction, Trans. Math. Software, 24, 437–474, doi:10.1145/293686.293695, 1998.

Giles, M. B. and Pierce, N. A.: An introduction to the adjoint approach to design, Flow Turbul. Combust., 65, 393–415, 2000.

Gurney, K. R., Law, R. M., Denning, A. S., Rayner, P. J., Baker, D., Bousquet, P., Bruhwilerk, L., Chen, Y.-H., Ciais, P., Fan, S., Fung, I., Gloor, M., Heimann, M., Higuchi, K., John, J., Maki, T., Maksyutov, S., Masarie, K., Peylin, P., Prather, M., Pak, B. C., Randerson, J. R., Sarmiento, J., Taguchi, S., Takahashi, T., and Yuen, C.-W.: Towards robust regional estimates of CO_2 sources and sinks using atmospheric transport models, Nature, 415, 626–630, 2002.

Gurney, K. R., Law, R. M., Denning, A. S., Rayner, P. J., Pak, B. C., Baker, D., Bousquet, P., Bruhwiler, L., Chen, Y.-H., Ciais, P., Fung, I. Y., Heimann, M., John, J., Maki, T., Maksyutov, S., Peylin, P., Prather, M., and Taguchi, S.: Transcom 3 inversion intercomparison: model mean results for the estimation of seasonal carbon sources and sinks, Global Biogeochem. Cy., 18, GB1010, doi:10.1029/2003GB002111, 2004.

Hack, J. J., Boville, B. A., Briegleb, B. P., Kiehl, J. T., Rasch, P. J., and Williamson, D. L.: Description of the NCAR community climate model (CCM2), NCAR/TN-382, 108, 1993.

Haines, P. E., Esler, J. G., and Carver, G. D.: Technical Note: Adjoint formulation of the TOM-CAT atmospheric transport scheme in the Eulerian backtracking framework (RETRO-TOM), Atmos. Chem. Phys., 14, 5477–5493, doi:10.5194/acp-14-5477-2014, 2014.

Hayes, D. J., McGuire, A. D., Kicklighter, D. W., Gurney, K. R., Burnside, T. J., and Melillo, J. M.: Is the northern high-latitude land-based CO_2 sink weakening?, Global Biogeochem. Cy., 25, GB3018, doi:10.1029/2010GB003813, 2011.

Henze, D. K., Hakami, A., and Seinfeld, J. H.: Development of the adjoint of GEOS-Chem, Atmos. Chem. Phys., 7, 2413–2433, doi:10.5194/acp-7-2413-2007, 2007.

Hourdin, F. and Talagrand, O.: Eulerian backtracking of atmospheric tracers. I: Adjoint derivation and parametrization of subgid-scale transport, Q. J. Roy. Meteor. Soc., 132, 585–603, 2006.

IPCC: Climate change 2007: the physical science basis, in: Contribution of Working Group I to the Fourth Assessment Report of the Intergovernmental Panel on Climate Change, edited by: Solomon, S., Qin, D., Manning, M., Chen, Z., Marquis, M., Cambridge University Press, Cambridge, 135–145, 2007.

Ito, A.: Changing ecophysiological processes and carbon budget in East Asian ecosystems under near-future changes in climate: implications for long-term monitoring from a process-based model, J. Plant Res., 123, 577–588, 2010.

GMDD
8, 5983–6019, 2015

Kaminski, T., Heimann, M., and Giering, R.: A coarse grid three-dimensional global inverse model of the atmospheric transport: 1. Adjoint model and Jacobian matrix, J. Geophys. Res., 104, 18535–18553, doi:10.1029/1999JD900147, 1999a.

Kaminski, T., Heimann, M., and Giering, R.: A coarse grid three-dimensional global inverse model of the atmospheric transport: 2. Inversion of the transport of CO_2 in the 1980s, J. Geophys. Res., 104, 18555–18581, doi:10.1029/1999JD900146, 1999b.

Kaminski, T., Rayner, P., Heimann, M., and Enting, I.: On aggregation errors in atmospheric transport inversions, J. Geophys. Res., 106, 4703–4715, 2001.

Kuze, A., Suto, H., Nakajima, M., and Hamazaki, T.: Thermal and near infrared sensor for carbon observation Fourier-transform spectrometer on the Greenhouse Gases Observing Satellite for greenhouse gases monitoring, Appl. Optics, 48, 6716–6733, doi:10.1364/AO.48.006716, 2009.

Kopacz, M., Jacob, D. J., Henze, D. K., Heald, C. L., Streets, D. G., and Zhang, Q.: Comparison of adjoint and analytical Bayesian inversion methods for constraining Asian sources of carbon monoxide using satellite (MOPITT) measurements of CO columns, J. Geophys. Res., 114, D04305, doi:10.1029/2007JD009264, 2009.

Koyama, Y., Maksyutov, S., Mukai, H., Thoning, K., and Tans, P.: Simulation of variability in atmospheric carbon dioxide using a global coupled Eulerian – Lagrangian transport model, Geosci. Model Dev., 4, 317–324, doi:10.5194/gmd-4-317-2011, 2011.

Law, R. M., Rayner, P. J., Denning, A. S., Erickson, D., Fung, I. Y., Heimann, M., Piper, S. C., Ramonet, M., Taguchi, S., Taylor, J. A., Trudinger, C. M., and Watterson, I. G.: Variations in modelled atmospheric transport of carbon dioxide and the consequences for CO_2 inversions, Global Biogeochem. Cy., 10, 783–796, 1996.

Law, R. M., Peters, W., Rödenbeck, C., Aulagnier, C., Baker, I., Bergmann, D. J., Bousquet, P., Brandt, J., Bruhwiler, L., Cameron-Smith, P. J., Christensen, J. H., Delage, F., Denning, A. S., Fan, S., Geels, C., Houweling, S., Imasu, R., Karstens, U., Kawa, S. R., Kleist, J., Krol, M. C., Lin, S.-J., Lokupitiya, R., Maki, T., Maksyutov, S., Niwa, Y., Onishi, R., Parazoo, N., Patra, P. K., Pieterse, G., Rivier, L., Satoh, M., Serrar, S., Taguchi, S., Takigawa, M., Vautard, R., Vermeulen, A. T., and Zhu, Z.: TransCom model simulations of hourly atmospheric CO_2: experimental overview and diurnal cycle results for 2002, Global Biogeochem. Cy., 22, GB3009, doi:10.1029/2007GB003050, 2008.

Maki, T., Ikegami, M., Fujita, T., Hirahara, T., Yamada, K., Mori, K., Takeuchi, A., Tsutsumi, Y., Suda, K., and Conway, T. J.: New technique to analyse global distributions of CO_2 con-

GMDD
8, 5983–6019, 2015

centrations and fluxes from non-processed observational data, Tellus B, 62, 797–809, doi:10.1111/j.1600-0889.2010.00488.x, 2010.
Maksyutov, S., Patra, P. K., Onishi, R., Saeki, T., and Nakazawa, T.: NIES/FRCGC global atmospheric tracer transport model: description, validation, and surface sources and sinks inversion, J. Earth Simulator, 9, 3–18, 2008.
Maksyutov, S., Takagi, H., Valsala, V. K., Saito, M., Oda, T., Saeki, T., Belikov, D. A., Saito, R., Ito, A., Yoshida, Y., Morino, I., Uchino, O., Andres, R. J., and Yokota, T.: Regional CO_2 flux estimates for 2009–2010 based on GOSAT and ground-based CO_2 observations, Atmos. Chem. Phys., 13, 9351–9373, doi:10.5194/acp-13-9351-2013, 2013.
Marchuk, G.: Numerical Solution of the Problems of the Dynamics of the Atmosphere and the Ocean, Gidrometeoizdat, Leningrad, 303 pp., 1974 (in Russian).
Marchuk, G. I.: Adjoint Equations and Analysis of Complex Systems, Series: Mathematics and its Applications, v. 295, Kluwer Academic Publishers, Dordrecht and Boston, 484 pp., 1995.
McGuire, A. D., Anderson, L. G., Christensen, T. R., Dallimore, S., Guo, L. D., Hayes, D. J., Heimann, M., Lorenson, T. D., Macdonald, R. W., and Roulet, N.: Sensitivity of the carbon cycle in the Arctic to climate change, Ecol. Monogr., 79, 523–555, doi:10.1890/08-2025.1, 2009.
Meirink, J. F., Bergamaschi, P., Frankenberg, C., d'Amelio, M. T. S., Dlugokencky, E. J., Gatti, L. V., Houweling, S., Miller, J. B., Roeckmann, T., Villani, M. G., and Krol, M. C.: Four-dimensional variational data assimilation for inverse modeling of atmospheric methane emissions: analysis of SCIAMACHY observations, J. Geophys. Res., 113, D17301, doi:10.1029/2007JD009740, 2008.
Müller, J.-F. and Stavrakou, T.: Inversion of CO and NO_x emissions using the adjoint of the IMAGES model, Atmos. Chem. Phys., 5, 1157–1186, doi:10.5194/acp-5-1157-2005, 2005.
Oda, T. and Maksyutov, S.: A very high-resolution (1 km × 1 km) global fossil fuel CO_2 emission inventory derived using a point source database and satellite observations of nighttime lights, Atmos. Chem. Phys., 11, 543–556, doi:10.5194/acp-11-543-2011, 2011.
Onogi, K., Tsutsui, J., Koide, H., Sakamoto, M., Kobayashi, S., Hatsushika, H., Matsumoto, T., Yamazaki, N., Kamahori, H., Takahashi, K., Kadokura, S., Wada, K., Kato, K., Oyama, R., Ose, T., Mannoji, N., and Taira, R.: The JRA-25 reanalysis, J. Meteorol. Soc. Jpn., 85, 369–432, 2007.
Patra, P. K., Law, R. M., Peters, W., Rodenbeck, C., Takigawa, M., Aulagnier, C., Baker, I., Bergmann, D. J., Bousquet, P., Brandt, J., Bruhwiler, L., Cameron-Smith, P. J., Chris-

GMDD
8, 5983–6019, 2015

tensen, J. H., Delage, F., Denning, A. S., Fan, S., Geels, C., Houweling, S., Imasu, R., Karstens, U., Kawa, S. R., Kleist, J., Krol, M. C., Lin, S.-J., Lokupitiya, R., Maki, T., Maksyutov, S., Niwa, Y., Onishi, R., Parazoo, N., Pieterse, G., River, L., Satoh, M., Serrar, S., Taguchi, S., Vautard, R., Vermeulen, A. T., and Zhu, Z.: TransCom model simulations of hourly atmospheric CO_2: analysis of synoptic-scale variations for the period 2002–2003, Global Biogeochem. Cy., 22, GB4013, doi:10.1029/2007GB003081, 2008.

Patra, P. K., Houweling, S., Krol, M., Bousquet, P., Belikov, D., Bergmann, D., Bian, H., Cameron-Smith, P., Chipperfield, M. P., Corbin, K., Fortems-Cheiney, A., Fraser, A., Gloor, E., Hess, P., Ito, A., Kawa, S. R., Law, R. M., Loh, Z., Maksyutov, S., Meng, L., Palmer, P. I., Prinn, R. G., Rigby, M., Saito, R., and Wilson, C.: TransCom model simulations of CH_4 and related species: linking transport, surface flux and chemical loss with CH_4 variability in the troposphere and lower stratosphere, Atmos. Chem. Phys., 11, 12813–12837, doi:10.5194/acp-11-12813-2011, 2011.

Peters, W., Miller, J. B., Whitaker, J., Denning, A. S., Hirsch, A., Krol, M. C., Zupanski, D., Bruhwiler, L., and Tans, P. P.: An ensemble data assimilation system to estimate CO_2 surface fluxes from atmospheric trace gas observations, J. Geophys. Res., 110, D24304, doi:10.1029/2005JD006157, 2005.

Peters, W., Jacobson, A. R., Sweeney, C., Andrews, A. E., Conway, T. J., Masarie, K., Miller, J. B., Bruhwiler, L. M. P., Pétron, G., Hirsch, A. I., Worthy, D. E. J., van der Werf, G. R., Randerson, J. T., Wennberg, P. O., Krol, M. C., and Tans, P. P.: An atmospheric perspective on North American carbon dioxide exchange: carbonTracker, P. Natl. Acad. Sci. USA, 104, 18,925–18,930, doi:10.1073/pnas.0708986104, 2007.

Peylin, P., Rayner, P. J., Bousquet, P., Carouge, C., Hourdin, F., Heinrich, P., Ciais, P., and AEROCARB contributors: Daily CO_2 flux estimates over Europe from continuous atmospheric measurements: 1, inverse methodology, Atmos. Chem. Phys., 5, 3173–3186, doi:10.5194/acp-5-3173-2005, 2005.

Peylin, P., Law, R. M., Gurney, K. R., Chevallier, F., Jacobson, A. R., Maki, T., Niwa, Y., Patra, P. K., Peters, W., Rayner, P. J., Rödenbeck, C., van der Laan-Luijkx, I. T., and Zhang, X.: Global atmospheric carbon budget: results from an ensemble of atmospheric CO_2 inversions, Biogeosciences, 10, 6699–6720, doi:10.5194/bg-10-6699-2013, 2013.

Rayner, P. J. and O'Brien, D. M.: The utility of remotely sensed CO_2 concentration data in surface source inversions, Geophys. Res. Lett., 28, 175–178, 2001.

GMDD
8, 5983–6019, 2015

Rigby, M., Manning, A. J., and Prinn, R. G.: Inversion of long-lived trace gas emissions using combined Eulerian and Lagrangian chemical transport models, Atmos. Chem. Phys., 11, 9887–9898, doi:10.5194/acp-11-9887-2011, 2011.

Rodgers, C. D.: Inverse Methods for Atmospheric Sounding, vol. 2 of Series on Atmospheric, Oceanic and Planetary Physics, World Scientific, Singapore, 2000.

Rödenbeck, C., Houweling, S., Gloor, M., and Heimann, M.: Time-dependent atmospheric CO_2 inversions based on interannually varying tracer transport, Tellus B, 55, 488–497, 2003.

Rödenbeck, C., Gerbig, C., Trusilova, K., and Heimann, M.: A two-step scheme for high-resolution regional atmospheric trace gas inversions based on independent models, Atmos. Chem. Phys., 9, 5331–5342, doi:10.5194/acp-9-5331-2009, 2009.

Saito, M., Ito, A., and Maksyutov, S.: Evaluation of biases in JRA-25/JCDAS precipitation and their impact on the global terrestrial carbon balance, J. Climate, 24, 4109–4125, 2011.

Saito, M., Ito, A., and Maksyutov, S.: Optimization of a prognostic biosphere model for terrestrial biomass and atmospheric CO_2 variability, Geosci. Model Dev., 7, 1829–1840, doi:10.5194/gmd-7-1829-2014, 2014.

Saeki, T., Maksyutov, S., Sasakawa, M., Machida, T., Arshinov, M., Tans, P., Conway, T. J., Saito, M., Valsala, V., Oda, T., Andres, R. J., and Belikov, D.: Carbon flux estimation for Siberia by inverse modeling constrained by aircraft and tower CO_2 measurements, J. Geophys. Res.-Atmos., 118, 1100–1122, doi:10.1002/jgrd.50127, 2013.

Sasakawa, M., Shimoyama, K., Machida, T., Tsuda, N., Suto, H., Arshinov, M., Davydov, D., Fofonov, A., Krasnov, O., Saeki, T., Koyama, Y., and Maksyutov, S.: Continuous measurements of methane from a tower network over Siberia, Tellus B, 62, 403–416, 2010.

Stohl, A., Forster, C., Frank, A., Seibert, P., and Wotawa, G.: Technical note: The Lagrangian particle dispersion model FLEXPART version 6.2, Atmos. Chem. Phys., 5, 2461–2474, doi:10.5194/acp-5-2461-2005, 2005.

Stohl, A., Seibert, P., Arduini, J., Eckhardt, S., Fraser, P., Greally, B. R., Lunder, C., Maione, M., Mühle, J., O'Doherty, S., Prinn, R. G., Reimann, S., Saito, T., Schmidbauer, N., Simmonds, P. G., Vollmer, M. K., Weiss, R. F., and Yokouchi, Y.: An analytical inversion method for determining regional and global emissions of greenhouse gases: Sensitivity studies and application to halocarbons, Atmos. Chem. Phys., 9, 1597–1620, doi:10.5194/acp-9-1597-2009, 2009.

Takagi, H., Saeki, T., Oda, T., Saito, M., Valsala, V., Belikov, D., Saito, R., Yoshida, Y., Morino, I., Uchino, O., Andres, R. J., Yokota, T., and Maksyutov, S.: On the benefit of GOSAT observations to the estimation of regional CO_2 fluxes, SOLA, 7, 161–164, 2011.

Tans, P. P., Conway, T. J., and Nakazawa, T.: Latitudinal distribution of the sources and sinks of atmospheric carbon dioxide derived from surface observations and an atmospheric transport model, J. Geophys. Res., 94, 5151–5172, 1989.

Tarantola, A.: Inverse Problem Theory and Methods for Model Parameter Estimation, Society for Industrial and Applied Mathematics, Philadelphia, USA, 2005.

Thompson, R. L. and Stohl, A.: FLEXINVERT: an atmospheric Bayesian inversion framework for determining surface fluxes of trace species using an optimized grid, Geosci. Model Dev., 7, 2223–2242, doi:10.5194/gmd-7-2223-2014, 2014.

Valsala, V. and Maksyutov, S.: Interannual variability of the air–sea CO_2 flux in the north Indian Ocean, Ocean Dynam., 63, 165–178, doi:10.1007/s10236-012-0588-7, 2013.

van der Werf, G. R., Randerson, J. T., Giglio, L., Collatz, G. J., Mu, M., Kasibhatla, P. S., Morton, D. C., DeFries, R. S., Jin, Y., and van Leeuwen, T. T.: Global fire emissions and the contribution of deforestation, savanna, forest, agricultural, and peat fires (1997–2009), Atmos. Chem. Phys., 10, 11707–11735, doi:10.5194/acp-10-11707-2010, 2010.

Wilson, C., Chipperfield, M. P., Gloor, M., and Chevallier, F.: Development of a variational flux inversion system (INVICAT v1.0) using the TOMCAT chemical transport model, Geosci. Model Dev., 7, 2485–2500, doi:10.5194/gmd-7-2485-2014, 2014.

Yokota, T., Yoshida, Y., Eguchi, N., Ota, Y., Tanaka, T., Watanabe, H., and Maksyutov, S.: Global concentrations of CO_2 and CH_4 retrieved from GOSAT: first preliminary results, SOLA, 5, 160–163, doi:10.2151/sola.2009-041, 2009.

GMDD
8, 5983–6019, 2015

Table 1. The coupled model setups analyzed in this study.

Case	Resolution, °		Flux combination
	NIES TM	FLEXPART	
Cs-1	10.0	1.0	VISIT + CDIAC + OTTM
Cs-2	2.50	1.0	VISIT + CDIAC + OTTM
Cs-3	1.25	1.0	VISIT + CDIAC + OTTM

GMDD
8, 5983–6019, 2015

Table 2. Tower network sites in Siberia (JR-STATION).

Identifying code	Location	Latitude	Longitude	Sampling height (m)
DEM	Demyanskoe	59°47′29″	70°52′16″	63
IGR	Igrim	63°11′25″	64°24′56″	47
KRS	Karasevoe	58°14′44″	82°25′28″	67
NOY	Noyabrsk	63°25′45″	75°46′48″	43
SVV	Savvushka	51°19′30″	82°07′40″	52
VGN	Vaganovo	54°29′50″	62°19′29″	85
YAK	Yakutsk	62°05′19″	129°21′21″	77

GMDD
8, 5983–6019, 2015

Table 3. Information on the correlation coefficients, mean bias, and standard deviations between simulations using the coupled (Eulerian alone) model and observations.

Site	# of obs.	Cs-1 Correlation coefficient	Mean bias, ppm	SD, ppm	Cs-2 Correlation coefficient	Mean bias, ppm	SD, ppm	Cs-3 Correlation coefficient	Mean bias, ppm	SD, ppm
DEM	304	0.85 (0.85)	2.92 (3.68)	4.19 (4.37)	0.86 (0.84)	1.27 (2.03)	4.01 (4.37)	0.87 (0.84)	0.69 (1.45)	4.02 (4.27)
IGR	576	0.84 (0.87)	2.08 (2.72)	6.51 (7.27)	0.86 (0.86)	1.01 (1.66)	6.2 (7.13)	0.86 (0.85)	0.58 (1.23)	6.16 (7.07)
KRS	509	0.88 (0.9)	1.04 (1.44)	5.57 (6.66)	0.90 (0.91)	−0.05 (0.36)	4.92 (5.95)	0.91 (0.91)	−0.63 (−0.23)	4.79 (5.79)
NOY	382	0.86 (0.87)	1.48 (2.04)	5.24 (5.72)	0.90 (0.9)	0.07 (0.63)	4.51 (5.08)	0.91 (0.91)	−0.45 (0.12)	4.37 (4.9)
SVV	394	0.89 (0.88)	0.44 (0.16)	6.56 (7.62)	0.91 (0.88)	0.34 (0.06)	5.72 (6.74)	0.90 (0.88)	0.01 (−0.27)	5.6 (6.6)
VGN	609	0.88 (0.9)	1.49 (1.69)	5.04 (5.74)	0.91 (0.9)	0.62 (0.82)	4.36 (5.13)	0.91 (0.9)	0.25 (0.45)	4.23 (5.01)
YAK	405	0.84 (0.87)	1.22 (2.44)	5.37 (5.12)	0.86 (0.87)	−0.28 (0.94	5.68 (4.64)	0.85 (0.86)	−0.81 (0.42)	5.95 (4.74)
Average		0.86 (0.88)	1.52 (2.02)	5.50 (6.07)	0.89 (0.88)	0.43 (0.93)	5.06 (5.58)	0.89 (0.88)	−0.05 (0.45)	5.02 (5.48)

GMDD
8, 5983–6019, 2015

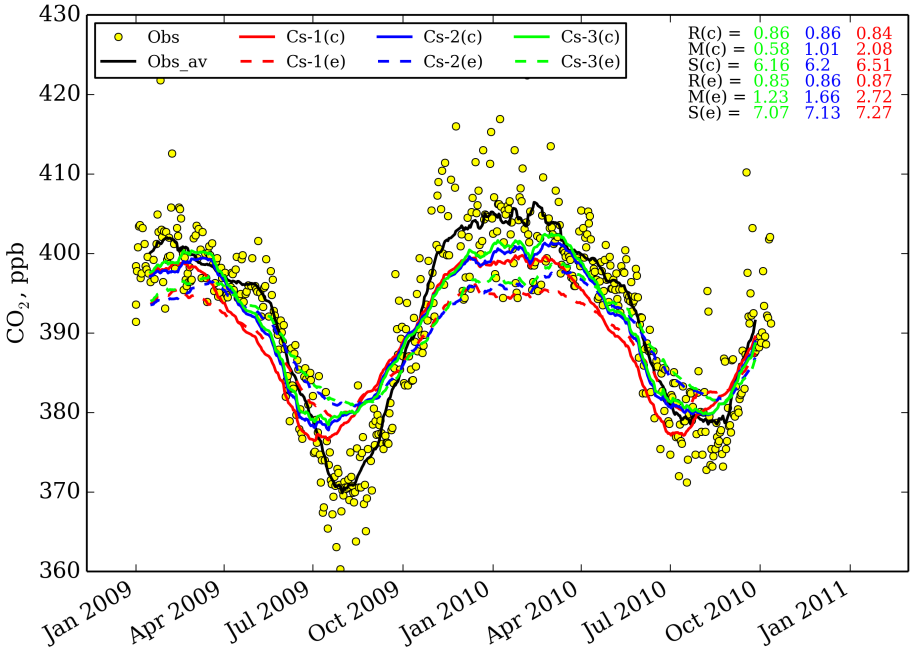

Figure 1. CO_2 mixing ratios observed at the Igrim tower, and simulated using the coupled ("c"; solid line) and Eulerian-only ("e"; dotted line) models using the model setups from Table 1 for 2009–2010. Symbols show individual observations; lines depict the moving average. Here, *r*, *s*, *m* mean the Pearson correlation, standard deviation and mean bias correspondently.

GMDD
8, 5983–6019, 2015

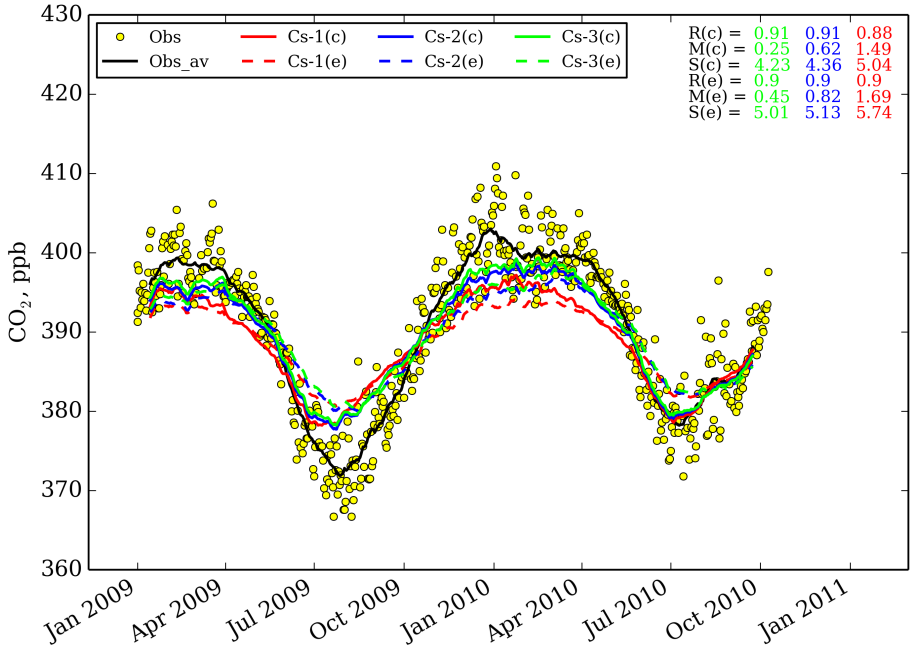

Figure 2. As for Fig. 2, but for the Vaganovo tower.

GMDD
8, 5983–6019, 2015

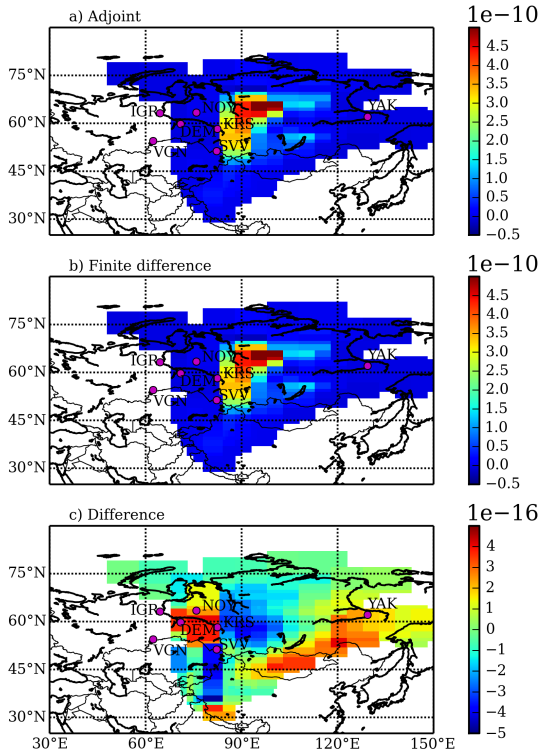

Figure 3. Comparison of sensitivities for test 1: **(a)** sensitivity calculated considering only the Eulerian adjoint model at a resolution of 2.5°, **(b)** the same sensitivity calculated directly from NIES forward runs using the one-sided numerical finite difference method with perturbations of ε, and **(c)** the difference between derived adjoint and numerical finite difference gradients. Magenta dots with labels depicts locations and names of Siberian observations towers.

GMDD
8, 5983–6019, 2015

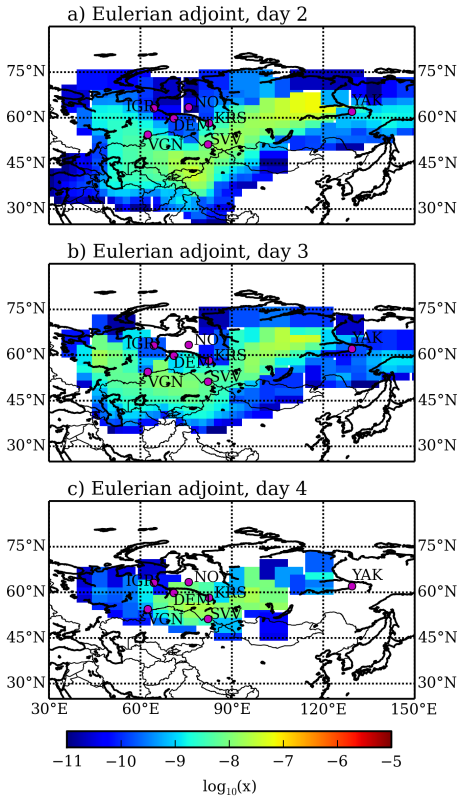

Figure 4. Sensitivities of CO_2 concentrations [ppm (μmol m^{-2} s^{-1})$^{-1}$] with respect to concentrations in adjacent cells, considering only the Eulerian adjoint model at a resolution of 2.5°.

GMDD
8, 5983–6019, 2015

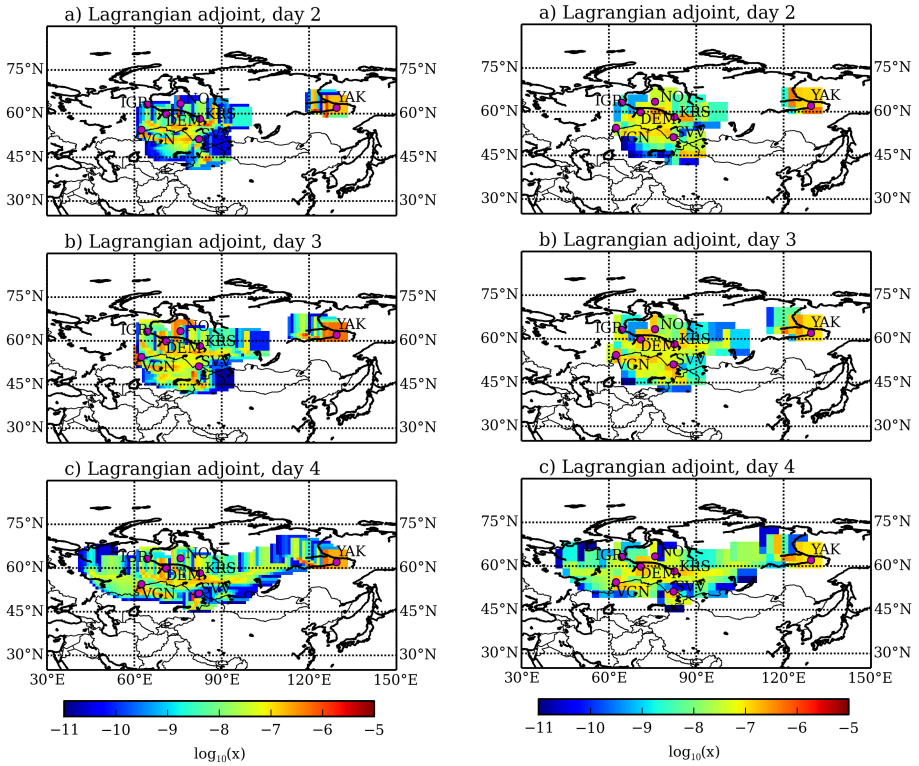

Figure 5. Same as Fig. 4, but considering only the Lagrangian adjoint model. The left panels show results on the native model grid with a resolution of 1.0°, while the right panels show the results aggregated on the grid at a resolution of 2.5°.

GMDD
8, 5983–6019, 2015

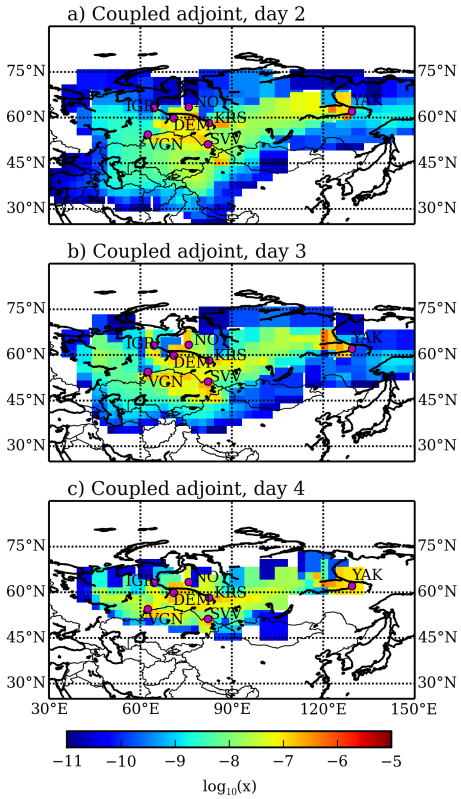

Figure 6. Same as Fig. 4, but considering the coupled adjoint model. Results from the Lagrangian adjoint model were aggregated on the grid of NIES TM at a resolution of 2.5°.

GMDD
8, 5983–6019, 2015

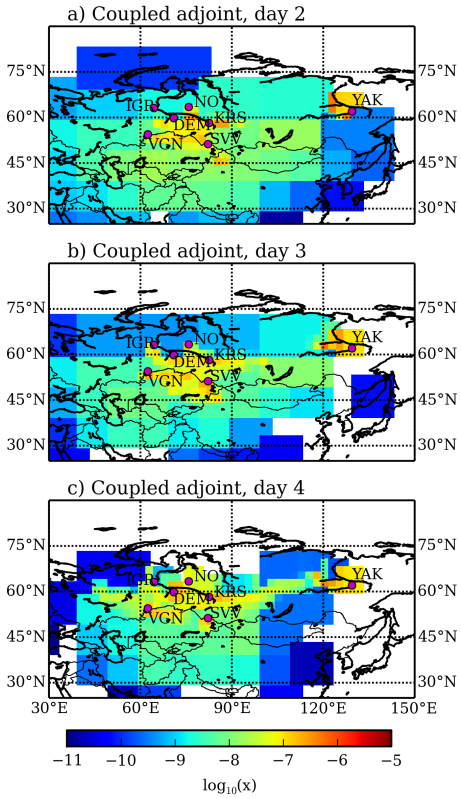

Figure 7. As for Fig. 6, but results from the Eulerian adjoint model were aggregated on the grid at a resolution of 10.0°.

GMDD
8, 5983–6019, 2015